J Therm Spray Tech
https://doi.org/10.1007/s11666-020-01051-4

PEER REVIEWED

Crystallinity, Stresses, and Cracks of YSZ Coatings Characterized by SEM–EBSD–Raman Spectroscopy

Xiao Zhu[1,2] · Yiling Huang[2] · Wei Zheng[2] · Jimei Zhang[2] · Chucheng Lin[2] · Christian Schwalb[3] · Yi Zeng[2]

Submitted: 8 February 2020 / in revised form: 30 April 2020

Abstract Yttria-stabilized zirconia (YSZ) thermal barrier coatings (TBCs) were prepared by atmospheric plasma spraying (APS). SEM–EBSD–Raman spectroscopy evaluated the relationship between the crystallinity, stresses, and cracks in YSZ coatings. Cracks were more likely to form in locations having poor crystallinity, due to the tensile stresses. Analysis between the formation of cracks and stresses shows that transgranular cracks are more likely created in areas with poor crystallinity. Moreover, intergranular cracks are more likely to occur around columnar grains, because the tensile stresses of columnar grains are greater than those of equiaxed grains. Resultantly, the formation and propagation of cracks can be controlled by controlling the cooling rate and grain shape.

Keywords cracks · grains · plasma spraying · Raman spectroscopy · residual stresses · YSZ coatings

✉ Yi Zeng
zengyi@mail.sic.ac.cn

[1] School of Materials Science and Engineering, University of Shanghai for Science and Technology, Shanghai 200093, China

[2] The State Key Lab of High Performance Ceramics and Superfine Microstructure, Shanghai Institute of Ceramics, Chinese Academy of Sciences, 1295 Dingxi Road, Shanghai 200050, China

[3] GETec Microscopy GmbH, Vienna, Austria

Introduction

Thermal barrier coatings (TBCs) are widely used in high-temperature components such as turbines and engines to protect these components from high-temperature oxidation and erosion, while improving the surface properties of the components, such as reliability and wear resistance (Ref 1–3). TBCs typically consist of a ceramic top coat, a metallic bond coat, and a substrate. The top coat, the most important component, is composed of yttria-stabilized zirconia (YSZ) because of its low thermal conductivity (approximately 2.3 W m^{-1} K^{-1} at 1000 °C) and high thermal expansion coefficient (11×10^{-6} °C) at high temperatures (Ref 4–6). YSZ TBCs are usually deposited by atmospheric plasma spraying (APS), because of its simplicity and efficiency (Ref 1). However, samples prepared by this process are greatly affected by residual stresses, which cause cracking and peeling of the coating (Ref 7).

Over the past few years, many studies have focused on the relationship between residual stresses and coatings. For instance, Jordan et al. used x-ray diffraction (XRD) to measure the change in stresses in different thermal cycles (Ref 8). Zhang et al. used a finite element analysis to prove that as the thickness of a coating increases, residual stresses appear as compressive stress and gradually decreases (Ref 9). Ma et al. calculated the stresses of the coating cross sections by Raman spectroscopy (Ref 10). Wang et al. used fluorescence spectra to characterize the stresses of YSZ/Al_2O_3 coatings and established the relationship between stresses and thickness density (Ref 11).

However, all of these approaches merely measure the stresses of coatings on the macroscale. On the microscale, Song et al. used electron backscattered diffraction (EBSD) and XRD to qualitatively compare the stresses of different

Published online: 21 May 2020

types of grains (Ref 12). However, no one has ever quantitatively calculated the stresses of the microstructure and grains. As is well known, the formation of cracks is closely related to stresses and can cause failure of the coating. If we can calculate the stresses of the coating microstructure, then we can determine which structures are more likely to cause crack formation. In addition, few researchers have studied the crystallinity of coatings, and there is a lack of advanced knowledge between the stresses and coating crystallinity.

In this work, YSZ TBCs were prepared by plasma spraying. The crystallinity and stresses of grains were characterized and calculated by scanning electron microscopy (SEM)–Raman spectroscopy and EBSD. Subsequently, the relationship between crystallinity, stresses, and cracks in YSZ coatings was analyzed in detail.

Experimental Procedure

Preparation of Coatings

In this experiment, vacuum plasma spraying (VPS; Sulzer Metco AG, Switzerland) was used to spray NiCrCoAlY powder on a nickel-based superalloy as a bonding layer. The ceramic layer was prepared by spraying ZrO_2-7.5 wt.% Y_2O_3 powder on the bonding layer by using atmospheric plasma spraying (APS; Sulzer Metco AG, Switzerland). The chemical composition of the Ni-based superalloy substrate is shown in Table 1. The VPS and APS parameters are listed in Table 2. The substrate was not preheated before plasma spraying and was cooled by compressed air during plasma spraying.

Characterization of Coatings

The microstructures of YSZ coatings were characterized by using an SEM system (Magellan 400, FEI, USA) equipped with EBSD (INCA SERIES, Oxford Instrument, UK) attachments. The EBSD patterns were acquired at an angle of 60° with an acceleration voltage of 20 kV; the step size was 0.1 μm for the sample. The stresses of the coating were characterized by SEM (Sigma 300, Zeiss, DEU) (MIRA3, TESCAN, CZ) equipped with Raman microscope probe attachments (RISE, WITEC, EU).

Raman Spectroscopy and Calculation of Residual Stresses

Raman spectroscopy is used not only for phase identification, but also for analysis of stresses. In this experiment, a green laser (wavelength 532 nm) was used as the laser light source, and the laser was incident perpendicular to the cross section of the coating. The spatial resolution of the instrument was spot size 700 nm, laser depth 1 μm, and grating 600 g/mm. The area of the Raman characterization was 35 × 25 mm^2, and the step size of the Raman characterization was 0.25 mm.

The change in stresses appears as a band shift of the peak in the Raman spectrum. The reason is that the change in stresses causes a change in the lattice parameters, which causes the peak position to move (Ref 13–16). As shown in Table 3, tetragonal zirconia generally has six peaks. The peaks at the positions of 460 cm^{-1} or 635 cm^{-1} are generally selected to calculate the stresses of ZrO_2 (Ref 17–20), because the peaks at 460 cm^{-1} are more sensitive to the change in stresses, and the peaks at 635 cm^{-1} have a better signal-to-noise (*S*/*N*) ratio (Ref 21, 22). In this experiment, we selected the peak near 635 cm^{-1} for calculation of stresses. The obtained Raman data were fitted and processed by the software PROJECT5 in the RISE system.

The relationship between residual stresses (σ_r) and Raman peak band shift (ΔV) is written as

$$\Delta V = \Pi_u \sigma_r \quad \text{(Eq 1)}$$

where the piezoelectric spectral coefficient Π_u is constant. The Π_u value for plasma-sprayed TBC was found to be 25 cm^{-1}/GPa (Ref 10).

Results and Discussion

Characterization of the Coatings

Figure 1(a) shows typical SEM images of the polished cross sections of YSZ coatings, from which we observe that the coating has some pores and cracks. Figure 1(b) shows the Raman mapping, and Fig. 1(c) shows its corresponding spectrum. (The green spectrum in Fig. 1(c) corresponds to the green area in Fig. 1(b), as does the yellow one.) The peak below 700 cm^{-1} in Fig. 1(c) is the peak of the sample, and the peak at 1500 cm^{-1} is the carbon peak. The carbon peak has no effect on the sample

Table 1 Chemical composition of Ni-based superalloy substrate

Composition	Ni	Cr	Mo	Co + Ta	Fe	Ti	Al	C	Mn	S	Si	P
Content (wt.%)	60.287	22.0	9.0	3.5	4.0	0.3	0.3	0.05	0.3	0.003	0.25	0.01

Table 2 Operating parameters used for plasma spraying

	Current, A	Ar, L/min	H_2, L/min	Powder feed rate, r/prm	Spray distance, mm
APS	600	26	11	25	120
VPS	720	50	9	25	275

Table 3 Wavenumber and symmetry of tetragonal zirconia peak

Wave number, cm^{-1}	148	258	318	470	610	635
Symmetry	B_1g	A_1g	B_1g	Eg	B_1g	Eg

wavenumbers into formula (1) yields a σ_r value of 108 MPa, which means the tensile stresses in the yellow region are 108 MPa greater than the tensile stresses in the green region. From this, we know that the yellow region has not only worse crystallinity but also greater tensile

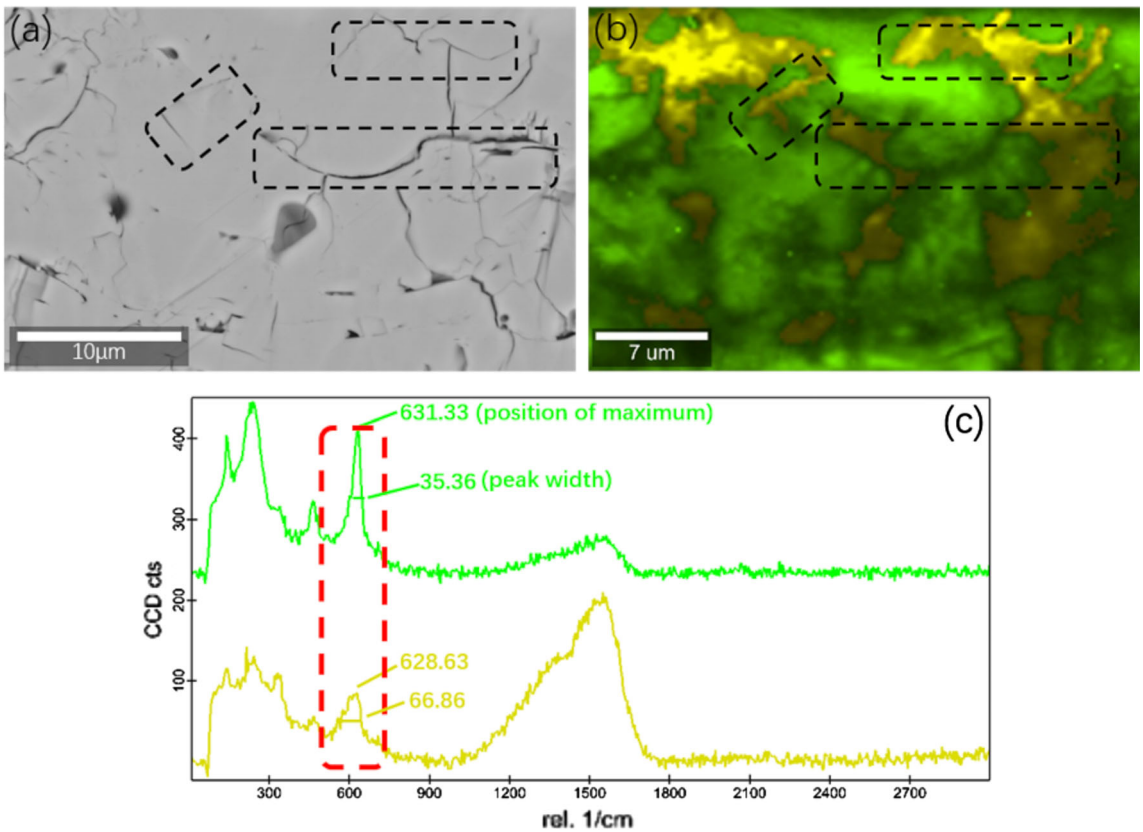

Fig. 1 (a) SEM image of a polished cross section of a YSZ coating, (b) image of Raman mapping, and (c) image of Raman spectrum

peaks. Comparing the two spectra in Fig. 1(c) with the standard zirconia spectrum shows that both spectra in Fig. 1(c) are tetragonal, but it is clear that there are some differences between the two spectra, such as the peak width and the position of the maximum. Comparing the peak width of the two spectra shows that the peak width of the green spectrum is significantly smaller than that of the yellow spectrum, which means that the crystallinity of the green region is better than that of the yellow region. At the same time, we also compared the Raman band shift of the two peaks at 635 cm^{-1}. The wavenumbers of the two spectra are 631.33 cm^{-1} and 628.63 cm^{-1}, and the band shift indicates a change in stresses. Substituting the two stresses compared to the green region. Comparing Fig. 1(b) with Fig. 1(a) shows that the yellow area is mainly concentrated near the crack; that is to say, where the crystallinity is poor, tensile stresses are greater and cracks are more likely to form.

At the same time, we speculated that the differences in crystallinity are caused by different cooling rates. According to the crystallization kinetics (Ref 23),

$$U = f\lambda v_0 \exp(-\Delta Ga/kT)[[1 - \exp(-V\Delta Gv/kT)] \quad \text{(Eq 2)}$$

where U is the growth rate of the crystal line, T is the temperature, ΔGa is the activation energy required for an

atom or molecule to transition from the liquid through the interface to the crystal, f is the additional factor, v_0 is the atomic vibration frequency, λ is the atomic distance, and $V\Delta Gv$ is the free enthalpy difference between the liquid and the crystal. The grain growth means the movement of interface. When the precipitated crystal has the same phase as the parent phase, the particles near the interface can be attached to the surface of the crystal nucleus through the transition of interface. So the crystal growth is controlled by the interface. If the precipitated crystal is different from the parent phase, the components of crystal would diffuse from parent phase to the interface before transition of the interface. Thus, the crystal growth is controlled by the diffusion. In this research, the phase of crystal is the same as parent phase. As a result, the main factor to determine the grain growth is the interface.

Figure 2 is obtained from formula 2 and shows that the crystal growth rate is mainly affected by temperature. When the cooling rate is fast, the crystallinity is poor, and when the cooling rate is slow, the crystallinity is better. The maximum value appears at an appropriate temperature.

We drew this process as a schematic diagram. As shown in Fig. 3, the coating was prepared by APS; during the cooling process, the cooling rate is different everywhere, so the crystal growth rate is also significantly different, which causes unequal crystallinity. It was calculated that the tensile stresses are greater where the crystallinity is poor, so it is easier to form cracks in the area with poor crystallinity.

Characterization of the Cracks

We performed EBSD on the selected area in Fig. 4(a), and the results are shown in Fig. 4(b). Figure 4(b) shows that some of the cracks are transgranular and others are intergranular.

In Fig. 5(a) and (b), the marked grains are columnar grains (aspect ratio > 2). The figure shows that a transgranular crack exists in this grain, and the crystallinity in this grain is also uneven. We speculate that the reason for the transgranular crack is that the crystallinity of the single grains is not uniform, and the tensile stresses are greater where the crystallinity is poor, which causes more dislocations. The increasing dislocations generate a large number of slip bands, which reduces the grain strength and eventually causes transgranular cracks in places with poor crystallinity.

Fig. 2 Diagram of crystal growth rate vs. temperature

In Fig. 5(c) and (d), the cracks marked are intergranular cracks. Intergranular cracks are not concentrated in areas with poor crystallinity, because the grain boundary strength is relatively poor. After observation and statistics, we found that grain boundary cracks often occur around columnar grains.

In order to determine why intergranular cracks concentrate around columnar grains, we studied the stresses of different grains. As shown in Fig. 6(a), we selected five points in a single grain for the Raman spectroscopy test. The results obtained are shown in Fig. 6(b), and the average of wavenumber was used to calculate the stresses. We defined this grain as a zero-stress grain. After that, the wavenumbers of other grains were detected in the same way. From the obtained wavenumbers, we calculated the stresses of each grain; the results are shown in Fig. 6(c) and (d). It must be noted that the horizontally marked grains are equiaxed grains (aspect ratio < 2) and the vertically marked grains are columnar grains. From Fig. 6(d), we determine that the tensile stresses of columnar grains are greater than those of equiaxed grains, and this result perfectly explains why intergranular cracks concentrate around columnar grains.

At the same time, grain size affects the stresses. It is well known that small equiaxed grains stress has excellent mechanical properties. For the reason that the anisotropic of equiaxed grains is small, and plays a positive role in resisting the initiation and expansion of cracks (Ref 24–26). From Fig. 6(d), we figure out that large columnar grains have greater stresses than small equiaxed grains. As a result, intergranular cracks are more likely to occur at the large columnar grains.

Conclusion

In this study, YSZ TBCs were prepared by APS. SEM–EBSD–Raman spectroscopy was used to study the relationship between crystallinity, stresses, and cracks. The results are summarized as follows:

1. The crystallinity of the coating is uneven, stresses are concentrated in the areas with poor crystallinity, and the cracks are more likely to form in these areas.

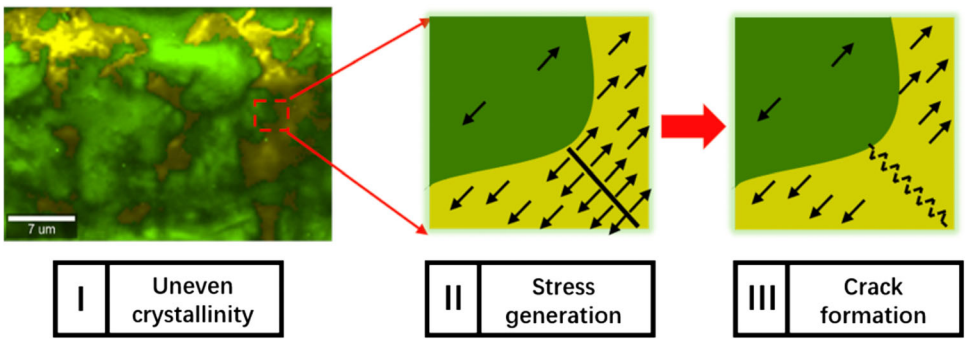

Fig. 3 Diagram of crack generation

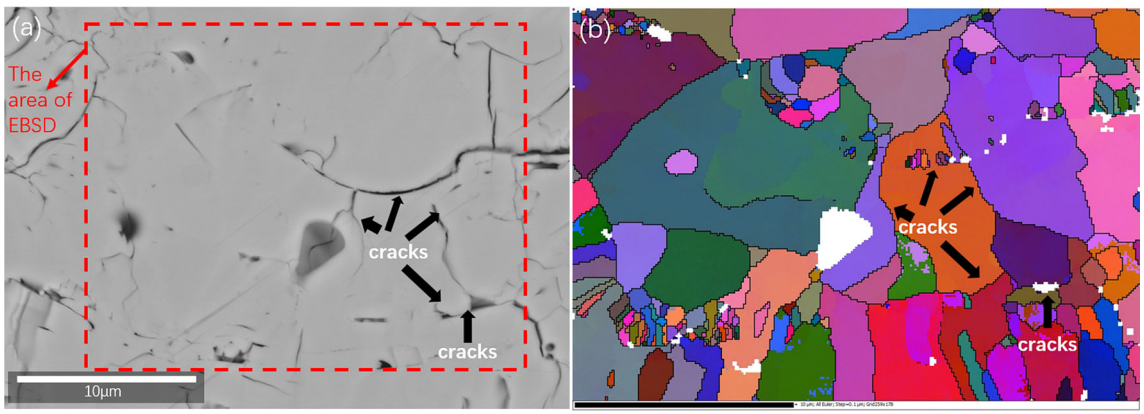

Fig. 4 (a) SEM images of polished cross sections; (b) EBSD orientation map of the corresponding area

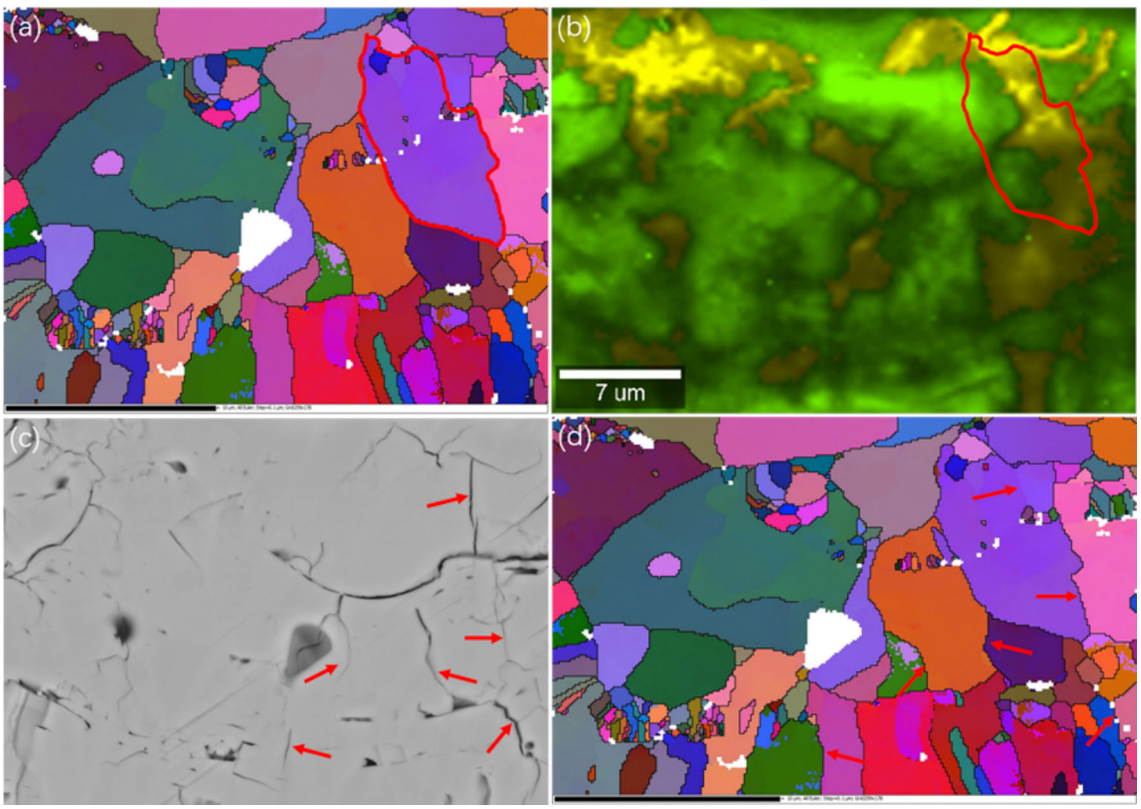

Fig. 5 (a, b) Transgranular crack in different images; (c, d) intergranular cracks in different images

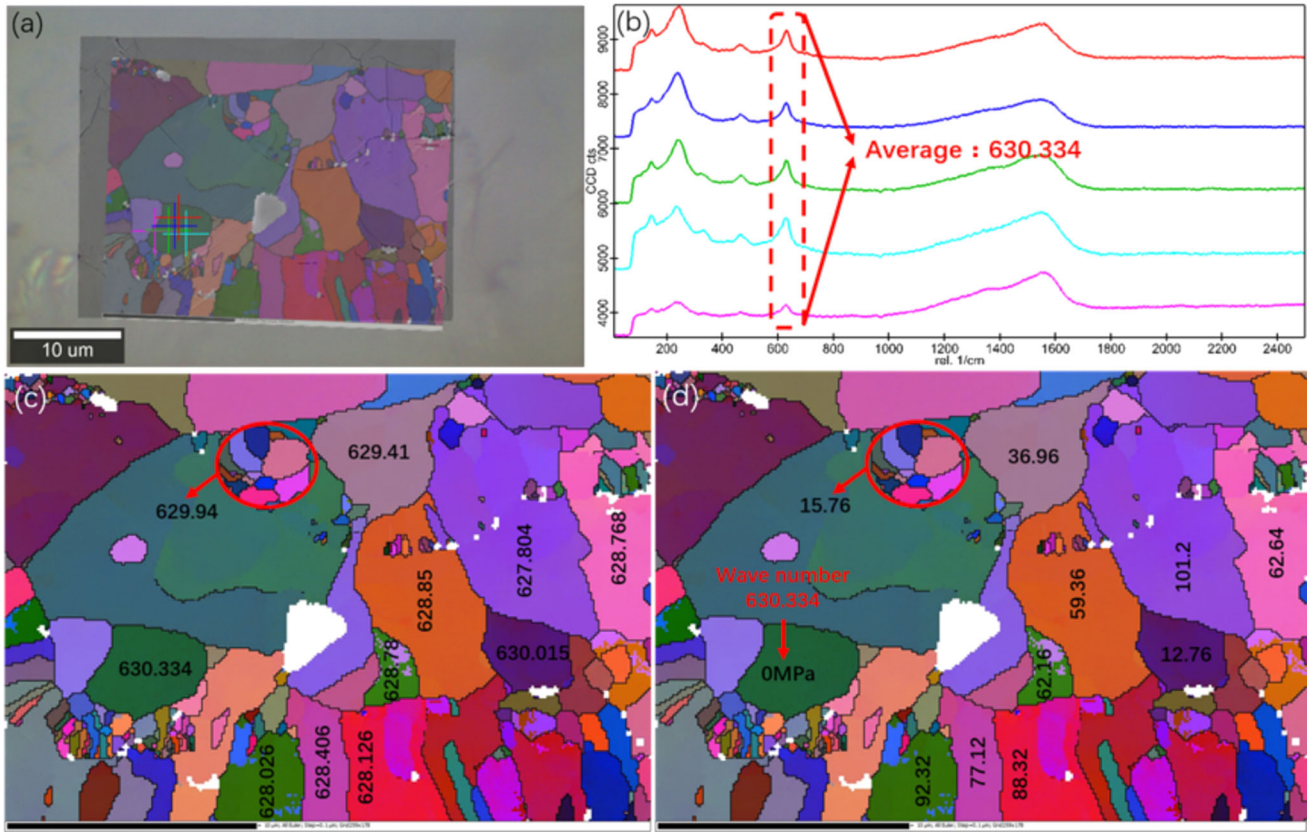

Fig. 6 (a) Location of the Raman test, (b) result of Raman test, (c) wavenumber of each grain, and (d) stresses of each grain

2. Transgranular cracks are more likely to occur in areas with poor crystallinity.
3. Intergranular cracks are more likely to occur at the columnar grains, because the tensile stresses of the columnar grains are greater than those of the equiaxed grains.

Acknowledgments The authors are grateful to the support provided by National Key R&D Program of China (2018YFB0704400), CAS Key Foundation for Exploring Scientific Instrument (YJKYYQ20170041), the Shanghai Sailing Program (18YF1427000), Shanghai Technical Platform for Testing on Inorganic Materials (19DZ2290700), the Research Project of Shanghai Science and Technology Committee (19142200600), International Partnership Program of Science (No. GJHZ1721), and National Nature Science Foundation of China (Grants 81101343, 51302170).

References

1. M.-J. Lee, B.-C. Lee, J.-G. Lim, and M.-K. Kim, Residual Stress Analysis of the Thermal Barrier Coating System by Considering the Plasma Spraying Process, *J. Mech. Sci. Technol.*, 2014, **28**(6), p 2161-2168
2. D.J. Quinn, B. Wardle, and S.M. Spearing, Residual Stress and Microstructure of As-deposited and Annealed, Sputtered Yttria-Stabilized Zirconia Thin Films, *J. Mater. Res.*, 2011, **23**(3), p 609-618
3. Y. Wang, G. Darut, X.-T. Luo, T. Poirier, J. Stella, H. Liao, and M.-P. Planche, Influence of Preheating Processes on the Microstructure of Laser Glazed YSZ Coatings, *Ceram. Int.*, 2017, **43**(5), p 4606-4611
4. Y. Bai, L. Zhao, J.J. Tang, S.Q. Ma, C.H. Ding, J.F. Yang, L. Yu, and Z.H. Han, Influence of Original Powders on the Microstructure and Properties of Thermal Barrier Coatings Deposited by Supersonic Atmospheric Plasma Spraying, Part II: Properties, *Ceram. Int.*, 2013, **39**(4), p 4437-4448
5. W.R. Chen, R. Archer, X. Huang, and B.R. Marple, TGO Growth and Crack Propagation in a Thermal Barrier Coating, *J. Therm. Spray Technol.*, 2008, **17**(5–6), p 858-864
6. Z. Fan, K. Wang, X. Dong, W. Duan, X. Mei, W. Wang, J. Cui, and J. Lv, Influence of Columnar Grain Microstructure on Thermal Shock Resistance of Laser Re-melted ZrO_2-7 wt.% Y_2O_3 Coatings and Their Failure Mechanism, *Surf. Coat. Technol.*, 2015, **277**, p 188-196
7. M. Tanaka, M. Hasegawa, A.F. Dericioglu, and Y. Kagawa, Measurement of Residual Stress in Air Plasma-Sprayed Y_2O_3–ZrO_2 Thermal Barrier Coating System Using Micro-Raman Spectroscopy, *Mater. Sci. Eng.*, 2006, **419**(1–2), p 262-268
8. D.W. Jordan and K.T. Faber, X-ray Residual Stress Analysis of a Ceramic Thermal Barrier Coating Undergoing Thermal Cycling, *Thin Solid Films*, 1993, **235**(1–2), p 137-141
9. H.S. Zhang, Y. Wei, and X.G. Chen, Effect of Top-Layer Thickness on Thermal-Shocking Property of Plasma-Spraying $Sm_2Zr_2O_7$/YSZ Thermal Barrier Coatings, *Adv. Mater. Res.*, 2011, **354–355**, p 53-56
10. Ma. R., Tan. Z., Kang. G., Residual Stress Measurement of Sic fiber/YSZ Composite Thermal Barrier Coating by Micro-Raman spectroscopy. *IOP Conf. Ser.: Mater. Sci. Eng.*, 2018, 397

11. X. Wang and P. Xiao, Residual Stresses and Constrained Sintering of YSZ/Al_2O_3 Composite Coatings, *Acta Mater.*, 2004, **52**(9), p 2591-2603
12. X. Song, J. Zhang, C. Lin, Z. Liu, C. Jiang, M. Kong, and Y. Zeng, Microstructures and Residual Strain/Stresses of YSZ Coatings Prepared by Plasma Spraying, *Mater. Lett.*, 2019, **240**, p 217-220
13. C. Wulfman, M. Sadoun, and M. Lamy de la Chapelle, Interest of Raman Spectroscopy for the Study of Dental Material: The Zirconia Material Example, *Irbm*, 2010, **31**(5–6), p 257-262
14. V. Teixeiraa. M. A., W. Fischerb, H.P. Buchkremerb, D. StoÈverb, Analysis of Residual Stresses in Thermal Barrier Coatings. *J. Mater. Process. Technol*., 1999 (92–93), p 209–216
15. P. Carpio, M.D. Salvador, A. Borrell, L. Navarro, and E. Sánchez, Molten Salt Attack on Multilayer and Functionally-Graded YSZ Coatings, *Ceram. Int.*, 2018, **44**(11), p 12634-12641
16. Y. Li, Y. Xie, L. Huang, X. Liu, and X. Zheng, Effect of Physical Vapor Deposited Al_2O_3 Film on TGO Growth in YSZ/CoNiCrAlY Coatings, *Ceram. Int.*, 2012, **38**(6), p 5113-5121
17. A.M. Limarga and D.R. Clarke, Piezo-Spectroscopic Coefficients of Tetragonal-Prime Yttria-Stabilized Zirconia, *J. Am. Ceram. Soc.*, 2007, **90**(4), p 1272-1275
18. D. Liu, O. Lord, and P.E. Flewitt, Calibration of Raman Spectroscopy in the Stress Measurement of Air-Plasma-Sprayed Yttria-Stabilized Zirconia, *Appl. Spectrosc.*, 2012, **66**(10), p 1204-1209
19. W.G. Mao, Q. Chen, C.Y. Dai, L. Yang, Y.C. Zhou, and C. Lu, Effects of Piezo-Spectroscopic Coefficients of 8 wt.% Y_2O_3 Stabilized ZrO_2 on Residual Stress Measurement of Thermal Barrier Coatings by Raman Spectroscopy, *Surf. Coat. Technol.*, 2010, **204**(21–22), p 3573-3577
20. G. Pezzotti and A.A. Porporati, Raman Spectroscopic Analysis of Phase-Transformation and Stress Patterns in Zirconia Hip Joints, *J. Biomed. Opt.*, 2004, **9**(2), p 372-384
21. L. Yang, F. Yang, Y. Long, Y. Zhao, X. Xiong, X. Zhao, and P. Xiao, Evolution of Residual Stress in Air Plasma Sprayed Yttria Stabilised Zirconia Thermal Barrier Coatings After Isothermal Treatment, *Surf. Coat. Technol.*, 2014, **251**, p 98-105
22. M. Tanaka, R. Kitazawa, T. Tomimatsu, Y.F. Liu, and Y. Kagawa, Residual Stress Measurement of an EB-PVD Y_2O_3-ZrO_2 Thermal Barrier Coating by Micro-Raman Spectroscopy, *Surf. Coat. Technol.*, 2009, **204**(5), p 657-660
23. Zhang. L., Huang. X., Song. X., *Crystal Growth Rate*, 2nd ed., Fundamentals of Materials Science, 2nd ed., Xu. Q., *Wuhan: Wuhan University of Technology Press*, 2008, p 423–426
24. Y. Wang, Y. Bai, K. Liu, J.W. Wang, and B.Q. Li, Microstructural Evolution of Plasma Sprayed Submicron-Nano-zirconia-Based Thermal Barrier Coatings, *Appl. Surf. Sci.*, 2015, **363**, p 101-112
25. J.B. Huang and W.Z. Wang, Effects of Particle Size on Pore Structure of Plasma-Splayed YSZ Coatings, *Surf. Technol.*, 2018, **47**(4), p 29-34
26. K.S. Kumar, H.V. Swygenhoven, and S. Suresh, Mechanical Behavior of Nanocrystalline Metals and Alloys, *Acta Mater.*, 2003, **51**(19), p 5743-5774